METALS

Pure iron grains are rare in the universe

Yuki Kimura,[1]* Kyoko K. Tanaka,[1] Takaya Nozawa,[2] Shinsuke Takeuchi,[3] Yuko Inatomi[3,4]

The abundant forms in which the major elements in the universe exist have been determined from numerous astronomical observations and meteoritic analyses. Iron (Fe) is an exception, in that only depletion of gaseous Fe has been detected in the interstellar medium, suggesting that Fe is condensed into a solid, possibly the astronomically invisible metal. To determine the primary form of Fe, we replicated the formation of Fe grains in gaseous ejecta of evolved stars by means of microgravity experiments. We found that the sticking probability for the formation of Fe grains is extremely small; only a few atoms will stick per hundred thousand collisions so that homogeneous nucleation of metallic Fe grains is highly ineffective, even in the Fe-rich ejecta of type Ia supernovae. This implies that most Fe is locked up as grains of Fe compounds or as impurities accreted onto other grains in the interstellar medium.

INTRODUCTION

Most of the atoms in the interstellar medium exist in the gas phase. Only about 1% of the total mass of the elements forms tiny solid particles called grains. Despite their low abundance, these grains are significant as building blocks of planetary systems (*1*), as substrates for the formation of molecules (*2*, *3*), as energy transducers in interstellar and circumstellar environments (*4*, *5*), and as key players in the efficient formation of stars (*6*, *7*). The efficiency of these various contributions depends strongly on the chemical composition, size, crystal structure, and geometry of the grains that are initially formed in gaseous outflows of evolved stars and subsequently processed in interstellar environments. Therefore, to understand these characteristics of grains, it is necessary first to clarify the compositions and quantities of grains formed in stellar gas outflows.

Iron (Fe) is a key element for deciphering the overall composition and amount of interstellar grains, because it is the most abundant refractory element in concurrence with magnesium and silicon in the cosmic abundance (*8*). Possible major components of Fe-rich grains include metallic iron, iron oxide, or iron sulfide (*9*). Fe-bearing grains are highly efficient catalysts for molecular formation (*10*). In addition, some Fe-bearing grains have high magnetic susceptibilities, and the resulting polarized thermal emissions and magnetic dipole emissions might efficiently disturb the cosmic microwave background (*11*). Therefore, the identification of the most common form of Fe is crucial in understanding the evolution history of grains, the reprocessing of electromagnetic waves, and the chemistry in the universe.

Despite extensive astronomical observations and analyses of meteorites, insufficient amounts of Fe compounds, including iron oxides, sulfides, and carbides, have been detected to account for the expected abundance of Fe in the universe (*12*–*14*), suggesting that most cosmic Fe atoms exist as grains of the pure metal. Therefore, the feasibility of the formation of metallic Fe grains in astronomical environments is an important subject for study. Here, we perform a reproduction experiment for the condensation of Fe grains in a model microgravity system, to elucidate the likelihood of the formation of Fe grains.

[1]Institute of Low Temperature Science, Hokkaido University, Sapporo 060-0819, Japan. [2]Division of Theoretical Astronomy, National Astronomical Observatory of Japan, Osawa 2-21-1, Mitaka, Tokyo 181-8588, Japan. [3]Institute of Space and Astronautical Science, Japan Aerospace Exploration Agency, 3-1-1 Yoshinodai, Chuo-ku, Sagamihara, Kanagawa 252-5210, Japan. [4]School of Physical Sciences, SOKENDAI (Graduate University for Advanced Studies), 3-1-1 Yoshinodai, Chuo-ku, Sagamihara, Kanagawa 252-5210, Japan.
*Corresponding author. Email: ykimura@lowtem.hokudai.ac.jp

RESULTS

Advantages of the microgravity experiment

Condensation of grains from the gas phase proceeds through the nucleation of stable small clusters and their subsequent growth. These processes are mainly controlled by two physical quantities: the sticking probability with which gas-phase atoms attach onto clusters or grains and the surface tension of small clusters. In most theoretical models of grain formation, the sticking probability has been assumed to be 1, and the surface tension has been assumed to equal that of the corresponding bulk material. However, this optimistic assumption regarding the sticking probability may lead to an overestimation of the grain formation rate; furthermore, the surface tension of particles with sizes of less than a few nanometers must differ markedly from the corresponding bulk value (*15*, *16*). To determine the physical quantities involved in the formation of Fe grains, we performed an ideal nucleation experiment in a microgravity environment of $(6.2 \pm 0.8) \times 10^{-3}$ m s^{-2} [$(6.3 \pm 0.8) \times 10^{-4}$ G] (fig. S1) aboard the sounding rocket S-520-28. An on-board in situ observation system composed of a nucleation chamber with a double-wavelength Mach-Zehnder–type laser interferometer and an image-recording system was adapted to conform to the size and weight limitations of the rocket (Fig. 1 and fig. S2) (*16*, *17*).

Nucleation experiments are conducted by observing the condensation of evaporated gas from a heated source in a buffer argon (Ar) gas. The Ar gas reduces the mean free path of the gas, thereby permitting a reduction in the physical scale of the experimental system. In ground-based experiments subject to the Earth's gravity, conditions for nucleation are not uniform because of the presence of thermal convection generated by the heated source. In a microgravity environment of the order of ~10^{-4} G, this thermal convection is fully suppressed, conferring the following three advantages. First, the evaporated hot gas diffuses isotropically, and the temperature profile around the evaporation source becomes concentric; consequently, nucleation occurs concentrically, as confirmed by microgravity experiments conducted in an aircraft (fig. S3). Second, the gases cool more slowly, and consequently, gaseous atoms can collide with each other more frequently on a longer time scale of gas cooling, providing a closer simulation of astronomical environments, such as the ejecta of supernovae or outflows from asymptotic giant branch stars. The nucleation process can be approximately described in terms of the product of the time scale for the supersaturation increase (τ_{sat}) and the collision frequency of iron atoms (ν); $\tau_{sat}\,\nu$ is about 10^3 to 10^4 for grain formation in supernovae and asymptotic giant branch stars (*18*, *19*). A similar value of $\tau_{sat}\,\nu$ of ~10^4 can be achieved in microgravity experiments (see Materials and Methods), whereas $\tau_{sat}\,\nu$ is

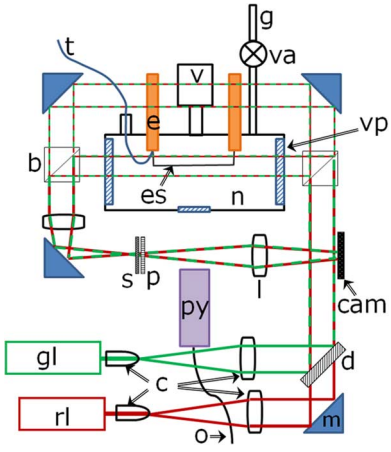

Fig. 1. Schematic of the configuration and optical path of the double-wavelength Mach-Zehnder–type laser interferometer with a nucleation chamber. The red and green lines show the optical paths of the red and green lasers, respectively. The resulting images of interference fringes are recorded with a charge-coupled device camera (cam). The evaporation source of Fe wire wrapped around a tungsten filament 0.3 mm in diameter and 68 mm in length is shown as the black solid line (es) in the nucleation chamber (n). The other labels are as follows: b, beam splitter; c, collimator; d, dichroic mirror; e, electrode; g, gas line; l, lens; m, mirror; o, optical fiber; p, polarizer; s, short-pass filter; t, thermocouple; v, vacuum gauge; gl, green laser; py, pyrometer; rl, red laser; va, valve; vp, view port.

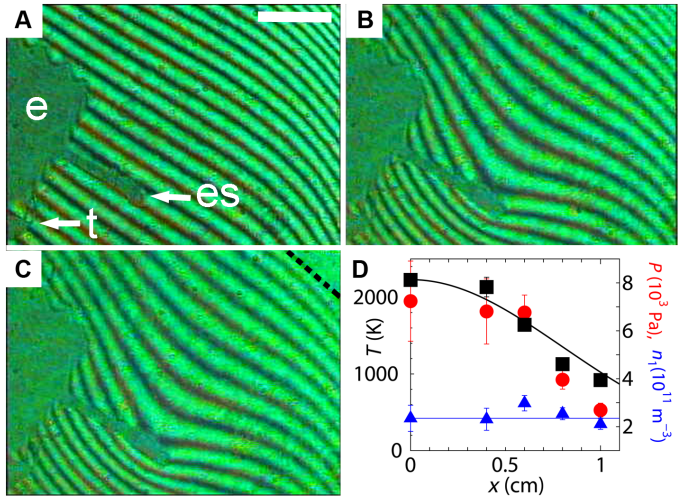

Fig. 2. Photographs of interference images and the temperature and partial pressure during the experiment on Fe nucleation under microgravity. Colored images of the interference fringes (see fig. S4 for monochromatic images) at representative times for the experiment with an initial pressure of Ar buffer gas of 4×10^4 Pa: (**A**) before heating of the evaporation source, (**B**) 0.4 s before the nucleation of Fe grains, and (**C**) at the time of nucleation. Scale bar, 3 mm. In (C), the dotted line in the upper right corner indicates the nucleation front of the Fe grains above which the disappearance of interference fringes is due to scattering of light by abundantly formed Fe grains. (**D**) Profiles of the temperature (squares), partial pressure (circles), and number density (triangles) of the Fe gas from the evaporation source to the nucleation front in (B). The error for the x axis is within the symbols. The solid black and blue curves are the temperature profile and the initial number density of Fe atoms, respectively, used in the calculation. The temperature was expressed by Eq. 10 with a time $t = x^2 D^{-1}$, where x is the distance from the evaporation source and D is the diffusion coefficient of Fe atoms. The labels are as follows: e, electrode; t, thermocouple; es, evaporation source.

only about 10^2 in ground-based experiments (*16*, *17*). Finally, the absence of thermal convection permits the reliable determination of physical quantities by comparison of the experimental results with values from the nucleation model. In ground-based experiments, the thermal convection supplies buffer gas continuously to the nucleation sites of grains, thereby complicating the interpretation of results.

Results of the microgravity experiment

In our microgravity experiments, the temperature and partial pressure of the Fe gas were determined simultaneously by observing shifts in the interference fringes of two lasers emitting polarized green (532 nm) and red (635 nm) lights (Fig. 2, A to C, and fig. S4). When the Fe evaporation source was electrically heated on a tungsten filament, the initial interference fringes in Fig. 2A were shifted because of a decrease in the refractive index of the warmed Ar buffer gas that filled the chamber at an initial pressure of 4.0×10^4 Pa (for example, Fig. 2B). When the source temperature was increased to 2226 ± 22 K, the interference fringes in the upper right corner of Fig. 2C disappeared. Nucleation of Fe grains can be detected from this disappearance of interference fringes, which results from scattering of the incident laser light by the newly formed Fe grains. We define the position where this occurs as the nucleation front (indicated by the dotted line in Fig. 2C), at which Fe grains nucleate and grow immediately. The derived temperature and partial pressure of Fe gas at the nucleation front were 907 ± 20 K and $(2.23 \pm 0.27) \times 10^3$ Pa, respectively; the uncertainty in these values arose from inaccuracies in measurements of the shifts of the interference fringes (see Materials and Methods). The temperature and partial pressure of Fe just before the nucleation decreased smoothly from the evaporation source to the nucleation front, whereas the number density of Fe was constant (Fig. 2D).

To examine the effects of Ar buffer gas, we performed an additional experiment at a reduced Ar pressure of 2.0×10^4 Pa. The temperature and partial pressure of Fe at the nucleation front were 958 ± 37 K and $(1.44 \pm 0.29) \times 10^3$ Pa, respectively, with an elevated source temperature of 2188 K.

Figure 3A shows the temperatures and partial pressures of Fe gas at the nucleation front determined from the experiments. In the case of an initial Ar gas pressure of 4.0×10^4 Pa, the nucleation temperature of Fe grains (907 K) was significantly below the solid-vapor equilibrium temperature (2116 K) corresponding to the partial pressure of Fe [$(2.23 \pm 0.27) \times 10^3$] at the nucleation front (Fig. 3B). Therefore, the degree of supercooling is as much as 1209 K. Because the equilibrium vapor pressure between gaseous and solid Fe at 907 K is 3.1×10^{-11} Pa, an extremely high supersaturation ratio of 7.2×10^{13} is realized at the nucleation front. For the experiment at an initial Ar gas pressure of 2.0×10^4 Pa, the resulting supersaturation ratio was 2.4×10^{12} based on the equilibrium vapor pressure between solid and vapor at the nucleation temperature of 958 K.

Determination of the physical properties

By applying nucleation theory, we determined the sticking probability α for Fe grain formation to explain the nucleation temperature obtained in the experiments. We used a semiphenomenological (SP) model, in which the formation energy of a cluster in the classical nucleation theory (CNT) is corrected for the binding energy of dimers (see Materials and Methods). In our calculations for grain formation, we defined the nucleation temperature as the point at which half the initial gas-phase Fe atoms have been consumed, because nucleation was detected

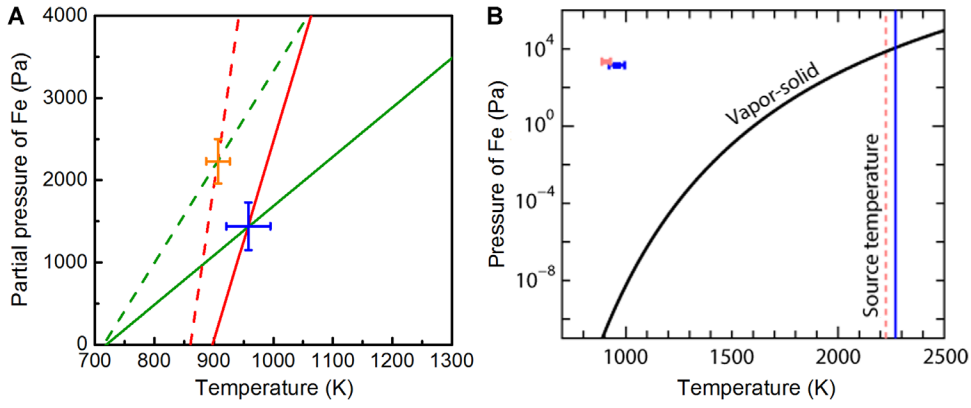

Fig. 3. Temperatures and partial pressures of Fe gas at the nucleation front, obtained from the microgravity experiments. (**A**) The blue and orange points with error bars indicate the temperatures and partial pressures of Fe gas just before the nucleation for the experiments at initial Ar gas pressures of 2.0×10^4 Pa and 4.0×10^4 Pa, respectively. The green and red lines show the relationship between the temperature and the partial pressure of Fe gas to explain the shifts in the interference fringes for the green and red laser beams; the solid and dashed lines are the results for Ar gas at 2.0×10^4 Pa and 4.0×10^4 Pa, respectively. (**B**) The equilibrium vapor pressure of Fe between the vapor and solid is shown by the solid curve. The two square symbols are the same as the points in (A). The temperatures measured at the evaporation source are shown by the blue and orange vertical lines for experiments in Ar gas at 2.0×10^4 Pa and 4.0×10^4 Pa, respectively. The large gap between the two square symbols and the solid curve shows the presence of a very large supersaturation at nucleation.

experimentally from the scattering of laser light. Consequently, a significant fraction of the Fe gas had to be locked up in Fe grains. Figure 4A shows the result of a simulation with $\alpha = 1.8 \times 10^{-5}$ and the surface tension (σ) of bulk Fe (2.48 N m^{-1}) (*20*). As the gas cools, the nucleation rate increases markedly because of the increase in the supersaturation ratio. Consequently, the number density of the remaining Fe gas decreases, and the nucleation rate decreases rapidly. The nucleation rate reaches a maximum at 1012 K, and the nucleation temperature is calculated to be 907 K. Therefore, this model with $\alpha = 1.8 \times 10^{-5}$ reproduces the experimental results closely. By taking into account inaccuracies in temperature, the sticking probability of Fe at ~900 K is found to be 1.4×10^{-5} to 2.0×10^{-5}. The resulting sticking probability depends on the definition of the nucleation temperature; for example, $\alpha = 1.2 \times 10^{-5}$ when the nucleation temperature is defined as the point at which 10% of the initial gas atoms are consumed, or $\alpha = 1.2 \times 10^{-4}$ at 90% consumption. Note that the grain formation model with $\alpha = 1$ predicts a nucleation temperature of about 1750 K (Fig. 4A) and therefore cannot explain the experimental results.

We also examined the dependence of the results on the surface tension. Because the surface tension σ of nanometer-scale Fe particles is likely to differ several tens of percent from that of bulk Fe (2.48 N m^{-1}), we considered a wider range of values $\sigma = 1.0$ to 3.3 N m^{-1}. As shown in Fig. 4B, the variability of the sticking probability is small in the plausible range of surface tensions of Fe. As mentioned above, the supersaturation ratio is remarkably high for nucleation of Fe grains in our experiments. As a result, the size of critical nuclei, which is the minimum number of atoms present in a small cluster that can grow continuously and with thermodynamic stability, should be small and is actually the dimer, as can be evaluated by means of Eq. 14. The formation of dimers from isolated atoms is the largest barrier to grain formation, because the forming dimer dissociates into the gas phase using the excess energy from the bonding. Therefore, the formation energy of a cluster is mainly determined by the binding energy of the dimer rather than by the surface tension, leading us to conclude that the binding energy of the dimer, as well as the sticking probability, is crucial for homogeneous nucleation.

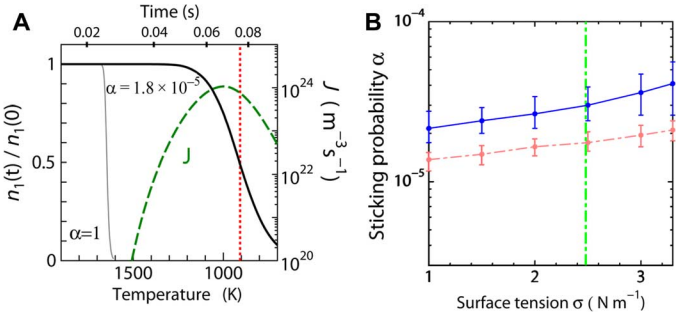

Fig. 4. Estimation of the sticking probability by simulations to explain the results of the experiments. (**A**) Result of calculations for the formation of Fe grains for a sticking probability of $\alpha = 1.8 \times 10^{-5}$ and a surface tension of σ = 2.48 N m^{-1}, which was obtained by applying the SP nucleation model. The dashed and solid curves show the time variation in the nucleation rate J and the number density of gas-phase Fe atoms $n_1(t)$, respectively. The vertical dotted line shows the nucleation temperature derived from microgravity experiments. The thin gray curve shows the number density of Fe atoms for $\alpha = 1$ and σ = 2.48 N m^{-1}, for which nucleation occurs at a much higher temperature (1700 K) than the experimental result. (**B**) Plot of the sticking probability α against the surface tension σ estimated from a comparison of the results of experiments and the simulations. The blue and orange points plot results for experiments in Ar gas at 2.0×10^4 Pa and 4.0×10^4 Pa, respectively. The vertical dot-dashed green line shows the bulk surface tension of molten Fe (*20*).

DISCUSSION

The extremely low sticking probability of Fe suggests that homogeneous nucleation of metallic Fe grains is highly inefficient. A similarly small sticking probability ($\alpha = \sim 10^{-5}$) has been reported for the formation of metallic zinc grains in a microgravity nucleation experiment (*21*). We have also measured a small sticking probability ($\alpha = 3.4 \times 10^{-5} \pm 1.2 \times 10^{-4}$) for metallic nickel grains in a microgravity experiment performed in an aircraft. In contrast, the sticking probability for the formation of grains including Fe in ground-based laboratory experiments is

significantly larger (α = ~10^{-2} to 1) (*16*, *22*). How then does gravity affect the sticking probability? One possibility is localized enhancement of gas density as a result of thermal convection; a higher density leads to a higher collision frequency of atoms, which might cause overestimation of the sticking probability. Another possibility is a heterogeneous effect; for example, small amounts of residual oxygen and water gas might be continuously supplied to the nucleation region by thermal convection. If seed nuclei of Fe oxides form rather than metallic Fe, atomic Fe might be able to stick to Fe oxides more efficiently than to metallic Fe.

The primary sources of cosmic Fe are considered to be type Ia supernovae, which are driven by thermonuclear fusion of white dwarfs (*23*). Iron atoms produced around the centers of type Ia supernovae are injected into the interstellar medium as cooling Fe-rich ejecta, in which Fe gas is believed to condense as pure Fe grains (*24*). However, despite the production of large quantities of Fe atoms, the formation of Fe grains has not yet been observed in type Ia supernovae (*25*). A theoretical model of grain formation shows that small amounts of Fe grains with a radius of 10 nm could form in type Ia supernovae if the sticking probability is assumed to be 1 (*26*). However, our results show that the sticking probability for the formation of Fe grains is extremely low, suggesting that homogeneous nucleation of Fe grains is much more difficult than previously expected. This explains why no metallic Fe grains have been observed in type Ia supernovae. In addition, the ejecta of type Ia supernovae are subjected to strong radiation fields for up to several hundred days after the explosion; the energetic photons and electrons could destroy small clusters, causing additional suppression of grain condensation.

If this is so, where in the universe is the Fe? Core-collapse supernovae arising from massive stars also produce Fe atoms and disperse them into the interstellar medium (*27*). It has been argued that an abundant mass of metallic Fe grains formed in the ejecta of supernova 1987A is required to explain the far-infrared flux observed by the Herschel Space Observatory (*28*). However, even if core-collapse supernovae synthesize Fe grains with high efficiency, we cannot conclude that cosmic Fe exists predominantly in the form of pure Fe grains because core-collapse supernovae are not the dominant source of Fe in the present universe (*27*). In addition, given the very low sticking probability determined from our experiments, Fe may not condense as the pure metal, but instead, it may condense onto other species of grains through heterogeneous nucleation. Many studies suggest that grains can grow through accretion of gas-phase atoms in interstellar environments, such as dense molecular clouds. In this case, it would be unnatural for Fe gas to accrete predominantly onto Fe grains rather than onto existing silicate or carbonaceous grains (*29*, *30*). Therefore, most of the Fe might be captured as impurities and/or components of other grains through physical and chemical processes in the interstellar medium.

MATERIALS AND METHODS

Determination of the temperature and partial pressure of Fe

In order to determine the partial pressure of evaporated Fe gas, we measured small changes in the refractive index by individually observing shifts in the interference fringes at two wavelengths. The refractive indices of Ar, $N_{\mathrm{Ar}(T,P)}$, and Fe, $N_{\mathrm{Fe}(T,P)}$, can be expressed as a function of the temperature T (K) and pressure P_{gas} (Pa), as follows

$$N_{\mathrm{gas}(T,P)} - 1 = \frac{\left[N_{\mathrm{gas}(273.15,P_0)} - 1\right]}{1 + a\Delta T}\frac{P_{\mathrm{gas}}}{P_0} \quad (1)$$

where a is the coefficient of volume expansion (0.003663 K^{-1} for Ar and 0.003661 K^{-1} for Fe in this experiment), $\Delta T = T - 273.15$ K, and pressure P_0 = 101,325 Pa. The values of $N_{\mathrm{Ar}} - 1$ are $(2.813 \pm 0.017) \times 10^{-5}$ and $(2.790 \pm 0.017) \times 10^{-5}$ at 532 and 632.8 nm, respectively, at 1.0×10^4 Pa and 293.15 K (*31*). The values of $N_{\mathrm{Fe}} - 1$ are 3.837×10^{-4} and 1.163×10^{-4} at 532 and 633 nm, respectively, at 2.0×10^4 Pa and 293 K (*32*).

The product of the shift in the fringes, Δd, and the wavelength of the laser, λ, are proportional to the change in the optical path length L, defined as $L = Nl$, where l is the physical length (taken to be the length of the tungsten filament, which was 68 mm, in this experiment). The shifts in the positions of the interference fringes for the green (Δd_{G}) and red lasers (Δd_{R}) after heating are given by the following equations

$$\Delta d_{\mathrm{G}} = \left[N_{\mathrm{G,Ar}(T_{\mathrm{i}},P_{\mathrm{i}})} - N_{\mathrm{G,Ar}(T,P-P_{\mathrm{Fe}})} - N_{\mathrm{G,Fe}(T,P_{\mathrm{Fe}})} + 1\right]\frac{l}{\lambda_{\mathrm{G}}} \quad (2)$$

and

$$\Delta d_{\mathrm{R}} = \left[N_{\mathrm{R,Ar}(T_{\mathrm{i}},P_{\mathrm{i}})} - N_{\mathrm{R,Ar}(T,P-P_{\mathrm{Fe}})} - N_{\mathrm{R,Fe}(T,P_{\mathrm{Fe}})} + 1\right]\frac{l}{\lambda_{\mathrm{R}}} \quad (3)$$

where T_{i} and P_{i} are the initial temperature and pressure, respectively, of Ar before the source temperature was elevated, and the subscripts G and R indicate quantities for the green and red lasers, respectively. Because the total pressure in the chamber P was monitored by using a pressure gauge, and Δd_{G} and Δd_{R} can be observed in the images, it was possible to determine the gas temperature (T) and the partial pressure of Fe (P_{Fe}) simultaneously by using Eqs. 1 to 3. The amounts of fringe shift at the nucleation front just before the nucleation were Δd_{G} = 6.5 and Δd_{R} = 6.4 for the experiment at an initial Ar gas pressure of 4×10^4 Pa.

Model and numerical simulation

To interpret the results of our experiments, we performed numerical simulations of the nonequilibrium condensation of Fe on the basis of nucleation theory (*18*, *33*), by applying an SP nucleation model, which is one of the most successful and useful models (*34*, *35*). The SP model modifies the CNT by adding extra terms for the formation energy of a cluster, obtained by using the second virial coefficient of the vapor. This model succeeded in achieving agreement with the nucleation rates derived from experimental data or from MD simulations for various materials (*34*–*37*). In homogeneous nucleation theory, the nucleation rate J (that is, the rate at which the stable nuclei are formed per volume) is expressed as follows

$$J = \left\{\sum_{i=1}^{\infty}\frac{1}{R^+(i)n_{\mathrm{e}}(i)}\right\}^{-1} \quad (4)$$

where $R^+(i)$ is the accretion rate from an i-mer (a cluster containing i atoms) to an $(i+1)$-mer. The equilibrium number density of i-mers $n_{\mathrm{e}}(i)$ is given by

$$n_{\mathrm{e}}(i) = \frac{P_{\mathrm{Fe}}}{kT}\exp\left(-\frac{\Delta G_i}{kT}\right) \quad (5)$$

where P_{Fe} is the partial pressure of Fe gas, k is the Boltzmann constant, and ΔG_i is the free energy associated with the formation of a cluster of size i from the gas phase. The accretion rate $R^+(i)$ is given by

$$R^+(i) = \alpha n_1 v_{th}\left(4\pi r_1^2 i^{\frac{2}{3}}\right) \quad (6)$$

where n_1 is the number density of Fe atoms, v_{th} is the thermal velocity of gas given by $\sqrt{kT/(2\pi m)}$, and α is the sticking probability. The radius of an atom r_1 is defined as $(3m/4\pi\rho_m)^{1/3}$, where m is the mass of an atom and ρ_m is the bulk density.

Because of the exponential dependence of the free energy on J, evaluation of the free energy ΔG_i is important. Here, we used values of ΔG_i given by an SP model. In the SP model, ΔG_i is expressed as

$$\Delta G_i = -(i-1)kT\ln S + \sigma A_1\left(i^{\frac{2}{3}} - 1\right) + A_2\left(i^{\frac{1}{3}} - 1\right) \quad (7)$$

where S ($= P_{Fe}/P_{Fe,e}$) is the supersaturation ratio, σ is the surface tension, A_1 is the surface area of a monomer, and A_2 is a correction term determined from the second virial coefficient. $P_{Fe,e}$ is the equilibrium vapor pressure of bulk Fe materials at a given temperature (Fig. 3B).

Although we have no experimental data on the second virial coefficient of refractory metals such as Fe, we can evaluate A_2 by using a relationship between the second virial coefficient and the chemical potential of a dimer. According to Tanaka *et al.* (*33*), A_2 is expressed as

$$A_2 = [-(2^{2/3} - 1)\sigma A_1 - E + \mu_V + \mu_R + \mu_T](2^{1/3} - 1)^{-1} \quad (8)$$

where E is the binding energy of a dimer and $\hbar$ is Planck's constant (*32*). In Eq. 8, μ_V, μ_R, and μ_T are the chemical potentials arising from vibrational, rotational, and translational motions of the dimers, as given by

$$\mu_V = kT\ln\left\{1 - \exp\left(-\frac{\hbar\omega}{kT}\right)\right\} + \frac{\hbar\omega}{2},\ \mu_R = -kT\ln\left(\frac{mR_e{}^2kT}{2\hbar^2}\right),$$

$$\mu_T = kT\ln\left\{\frac{P_{Fe,e}}{kT}\left(\frac{mkT}{4\pi\hbar^2}\right)^{-3/2}\right\} \quad (9)$$

where ω is the vibrational frequency of a dimer and R_e is the equilibrium distance between nuclei. Consequently, we can evaluate A_2 as a function of T for given σ, E, ω, and R_e. In our calculation, we adopted the values E/k = 8600 K, $\omega = 8.9 \times 10^{12}$ s^{-1}, and $R_e = 2.4 \times 10^{-10}$ m (*38*). In the SP model, the formation energy of a cluster is determined by the binding energy and chemical potentials arising from vibrational, rotational, and translational motions of dimers and the bulk surface tension. The formation energy for small clusters is primarily determined by the binding energy of the dimer rather than by the bulk surface tension, because the value of E is markedly dependent on the material. Note that the SP model gives the exact values of the free energy of monomer and dimer (ΔG_1 and ΔG_2), because $\Delta G_1 = 0$ is satisfied and ΔG_2 corresponds to the chemical potential of the dimer. There are large deviations from the values evaluated by CNT for clusters of fewer than about 10 atoms. Consequently, the correction term in ΔG_i is crucial for small clusters.

In the calculations, we consider a gaseous system containing Fe gas that cools with a characteristic time τ_T. In this case, the temperature T of the gas as a function of time t is given by

$$T(t) = T_0\exp(-t/\tau_T) \quad (10)$$

where T_0 is the initial temperature, which corresponded to the temperature of the heated source in our calculations (see below). As the gas temperature decreases, nucleation and grain growth proceed, consuming gas-phase Fe atoms. The number density of Fe gas $n_1(t)$ is given by

$$n_1(t) = n_1(0) - \int_0^t J(t')\left(\frac{r(t,t')}{r_1}\right)^3 dt' \quad (11)$$

where $J(t')$ is the nucleation rate at time t' and $r(t,t')$ is the radius of grains nucleated at t' and measured at t. The growth equation of a grain radius $r(t,t')$ is expressed in the form

$$\frac{\partial r(t,t')}{\partial t} = \alpha\frac{4\pi}{3}r_1^3 n_1(t)v_{th} \quad (12)$$

The radius of the critical nuclei $r(t,t')$ is

$$r(t,t') = i_*^{1/3}r_1 \quad (13)$$

where i_* is the number of atoms in the critical cluster, which is the smallest thermodynamically stable cluster and determined by $dn_e(i)/di = 0$; that is

$$i_* = \left(\frac{\sigma A_1 + \sqrt{(\sigma A_1)^2 + 3A_2kT\ln S}}{3kT\ln S}\right)^3 \quad (14)$$

By using Eqs. 4 to 14, which describe the nucleation rate and the nonequilibrium condensation, we simulated the condensation process of Fe by treating the sticking probability α and the surface tension σ as parameters.

In the calculations, we adopted initial partial pressures of Fe of $P_{Fe\ (t=0)}$ [$= n_1(0)kT$] = 1440 and 2230 Pa and initial temperatures of T_0 = 2188 and 2226 K for the experiments in Ar gas at initial pressures of 2.0×10^4 Pa and 4.0×10^4 Pa, respectively. The time scale for cooling τ_T was taken as the time required for the Fe gas to arrive at the nucleation site by diffusion from the evaporation source: $\tau_T \approx X^2D^{-1}$, where X is the distance from the evaporation source to the nucleation site ($X = 1.29 \times 10^{-2}$ m and 1.14×10^{-2} m) and $D = v_{mean}\lambda/3$ is the diffusion coefficient ($D = 3.07 \times 10^{-3}$ m^2 s^{-1} and 1.56×10^{-3} m^2 s^{-1}). Here, $v_{mean} = (8kT/\pi m)^{1/2}$ is the mean velocity of the gas (v_{mean} = 783 or 771 m s^{-1}), and $\lambda = (\sqrt{2}ns)^{-1}$ is the mean free path of a gas molecule ($\lambda = 1.18 \times 10^{-5}$ m or 6.06×10^{-6} m). The mean cross section of an Fe atom s is 4.988×10^{-20} m^2, and the number density of Ar gas n is 1.20×10^{24} m^{-3} (2.34×10^{24} m^{-3}) for the experiments in Ar gas at an initial pressure of 2.0×10^4 Pa (4.0×10^4 Pa), where we used the total gas pressures of 26,550 Pa (50,683 Pa), as measured in the experiments. The obtained time scale for cooling is $\tau_T = 5.42 \times 10^{-2}$ s and 8.33×10^{-2} s for the experiments in Ar gas at initial pressures of 2.0×10^4 Pa and 4.0×10^4 Pa,

respectively. In these estimations, we adopted the mean temperatures (1614 or 1567 K) between the evaporation source and the nucleation site. There is an uncertainty in the value of τ_T within a factor of 2 because τ_T is proportional to $T^{-3/2}$, leading to small deviations from the evaluated value of α to explain the experiments (within a factor of 2).

It is known that the nucleation process can be approximately described in terms of the product of the time scale for the supersaturation increase τ_{sat} and the collision frequency of iron atoms ν (*18*). The collision frequency of iron atoms ν was 2.52×10^6 s^{-1} or 3.96×10^6 s^{-1} for experiments in Ar gas at initial pressures of 2.0×10^4 Pa and 4.0×10^4 Pa, respectively. Because τ_{sat} was evaluated from $\tau_T kT/H$ with the latent heat ($H/k = 4.5 \times 10^4$ K), the corresponding values of τ_{sat} ν were calculated to be 4.9×10^3 and 1.1×10^4, which are similar to those in the grain formation environments of supernovae and asymptotic giant branch stars (*19*), whereas τ_{sat} ν was determined to be ~10^2 in ground-based experiments because of the smaller value of τ_T (~10^{-4} s) (*16*, *17*).

SUPPLEMENTARY MATERIALS

Supplementary material for this article is available at http://advances.sciencemag.org/cgi/content/full/3/1/e1601992/DC1

Supplementary Text

fig. S1. Time evolution of the acceleration gravity in the sounding rocket during the microgravity experiment.

fig. S2. Photographs of the experimental systems.

fig. S3. Examples of nucleated particles in a microgravity environment.

fig. S4. Images of interference fringes during the Fe nucleation experiment under microgravity.

REFERENCES AND NOTES

1. A. J. Weinberger, Planetary science: Construction-site inspection. *Nature* **433**, 114–115 (2005).
2. T. Hama, N. Watanabe, Surface processes on interstellar amorphous solid water: Adsorption, diffusion, tunneling reactions, and nuclear-spin conversion. *Chem. Rev.* **113**, 8783–8839 (2013).
3. J. A. Nuth III, N. M. Johnson, Complex protostellar chemistry. *Science* **336**, 424–425 (2012).
4. T. T. Takeuchi, V. Buat, D. Burgarella, The evolution of the ultraviolet and infrared luminosity densities in the universe at $0 < z < 1$. *Astron. Astrophys.* **440**, L17–L20 (2005).
5. W. A. Schutte, A. G. G. M. Tielens, Theoretical studies of the infrared emission from circumstellar dust shells: The infrared characteristics of circumstellar silicates and the mass-loss rate of oxygen-rich late-type giants. *Astrophys. J.* **343**, 369–392 (1989).
6. L. J. Tacconi, R. Genzel, R. Neri, P. Cox, M. C. Cooper, K. Shapiro, A. Bolatto, N. Bouché, F. Bournaud, A. Burkert, F. Combes, J. Comerford, M. Davis, N. M. Förster Schreiber, S. Garcia-Burillo, J. Gracia-Carpio, D. Lutz, T. Naab, A. Omont, A. Shapley, A. Sternberg, B. Weiner, High molecular gas fractions in normal massive star-forming galaxies in the young Universe. *Nature* **463**, 781–784 (2010).
7. C. F. McKee, Let there be dust. *Science* **333**, 1227–1228 (2011).
8. M. Asplund, N. Grevesse, A. J. Sauval, P. Scott, The chemical composition of the sun. *Annu. Rev. Astron. Astrophys.* **47**, 481–522 (2009).
9. A. P. Jones, Iron or iron oxide grains in the interstellar medium? *Mon. Not. R. Astron. Soc.* **245**, 331–334 (1990).
10. N. M. Johnson, M. McCarthy, J. A. Nuth III, Rate comparisons of magnetite and iron catalysts during Fischer-Tropsch-type reactions, in *Proceedings of the 45th Lunar and Planetary Science Conference,* The Woodlands, TX, 17 to 21 March 2014.
11. T. Hoang, A. Lazarian, Polarization of magnetic dipole emission and spinning dust emission from magnetic nanoparticles. *Astrophys. J.* **821**, 91 (2016).
12. J. Rho, W. T. Reach, A. Tappe, L. Rudnick, T. Kozasa, U. Hwang, M. Andersen, H. Gomez, T. DeLaney, L. Dunne, J. Slavin, Dust formation observed in young supernova remnants with Spitzer, in *ASP Conf. Ser. Vol. 414: Cosmic Dust: Near and Far*, T. Henning, E. Grün, J. Steinacker, Eds. (Astronomical Society of the Pacific, 2009), 22 pp.
13. A. M. Davis, Stardust in meteorites. *Proc. Natl. Acad. Sci. U.S.A.* **108**, 19142–19146 (2011).
14. T. K. Croat, F. J. Stadermann, T. J. Bernatowicz, Presolar graphite from AGB stars: Microstructure and *s*-process enrichment. *Astrophys. J.* **631**, 976–987 (2005).
15. H. Zhang, B. Chen, J. F. Banfield, The size dependence of the surface free energy of titania nanocrystals. *Phys. Chem. Chem. Phys.* **11**, 2553–2558 (2009).
16. Y. Kimura, K. K. Tanaka, H. Miura, K. Tsukamoto, Direct observation of the homogeneous nucleation of manganese in the vapor phase and determination of surface free energy and sticking coefficient. *Cryst. Growth Des.* **12**, 3278–3284 (2012).
17. Y. Kimura, H. Miura, K. Tsukamoto, C. Li, T. Maki, Interferometric in-situ observation during nucleation and growth of WO_3 nanocrystals in vapor phase. *J. Cryst. Growth* **316**, 196–200 (2011).
18. T. Yamamoto, H. Hasegawa, Grain formation through nucleation process in astrophysical environment. *Prog. Theor. Phys.* **58**, 816–828 (1977).
19. T. Nozawa, T. Kozasa, Formulation of non-steady-state dust formation process in astrophysical environments. *Astrophys. J.* **776**, 24 (2013).
20. H. L. Skriver, N. M. Rosengaard, Surface energy and work function of elemental metals. *Phys. Rev. B Condens. Matter Mater. Phys.* **46**, 7157–7168 (1992).
21. B. P. Michael, J. A. Nuth III, L. U. Lilleleht, Zinc crystal growth in microgravity. *Astrophys. J.* **590**, 579–585 (2003).
22. A. Giesen, A. Kowalik, P. Roth, Iron-atom condensation interpreted by a kinetic model and a nucleation model approach. *Phase Transitions* **77**, 115–129 (2004).
23. F. Matteucci, L. Greggio, Relative roles of type I and II supernovae in the chemical enrichment of the interstellar gas. *Astron. Astrophys.* **154**, 279–287 (1986).
24. E. Dwek, The evolution of the elemental abundances in the gas and dust phases of the galaxy. *Astrophys. J.* **501**, 643–665 (1998).
25. H. L. Gomez, C. J. R. Clark, T. Nozawa, O. Krause, E. L. Gomez, M. Matsuura, M. J. Barlow, M.-A. Besel, L. Dunne, W. K. Gear, P. Hargrave, Th. Henning, R. J. Ivison, B. Sibthorpe, B. M. Swinyard, R. Wesson, Dust in historical galactic type Ia supernova remnants with Herschel. *Mon. Not. R. Astron. Soc.* **420**, 3557–3573 (2012).
26. T. Nozawa, K. Maeda, T. Kozasa, M. Tanaka, K. Nomoto, H. Umeda, Formation of dust in the ejecta of type Ia supernovae. *Astrophys. J.* **736**, 45 (2011).
27. K. Nomoto, C. Kobayashi, N. Tominaga, Nucleosynthesis in stars and the chemical enrichment of galaxies. *Annu. Rev. Astron. Astrophys.* **51**, 457–509 (2013).
28. M. Matsuura, E. Dwek, M. Meixner, M. Otsuka, B. Babler, M. J. Barlow, J. Roman-Duval, C. Engelbracht, K. Sandstrom, M. Lakićević, J. Th. van Loon, G. Sonneborn, G. C. Clayton, K. S. Long, P. Lundqvist, T. Nozawa, K. D. Gordon, S. Hony, P. Panuzzo, K. Okumura, K. A. Misselt, E. Montiel, M. Sauvage, Herschel detects a massive dust reservoir in supernova 1987A. *Science* **333**, 1258–1261 (2011).
29. A. P. Jones, J. A. Nuth III, Dust destruction in the ISM: A re-evaluation of dust lifetimes. *Astron. Astrophys.* **530**, A44 (2012).
30. E. Dwek, Iron: A key element for understanding the origin and evolution of interstellar dust. *Astrophys. J.* **825**, 136 (2016).
31. Y. Clergent, C. Durou, M. Laurens, Refractive index variations for argon, nitrogen, and carbon dioxide at λ = 632.8 nm (He–Ne laser light) in the range 288.15 K ≤ *T* ≤ 323.15 K, 0 < *p* < 110 kPa. *J. Chem. Eng. Data* **44**, 197–199 (1999).
32. P. B. Johnson, R. W. Christy, Optical constants of transition metals: Ti, V, Cr, Mn, Fe, Co, Ni, and Pd. *Phys. Rev. B Condens. Matter Mater. Phys.* **9**, 5056–5070 (1974).
33. K. K. Tanaka, H. Tanaka, K. Nakazawa, Non-equilibrium condensation in a primordial solar nebula: Formation of refractory metal nuggets. *Icarus* **160**, 197–207 (2002).
34. A. Dillmann, G. E. A. Meier, A refined droplet approach to the problem of homogeneous nucleation from the vapor phase. *J. Chem. Phys.* **94**, 3872–3884 (1991).
35. A. Laaksonen, I. J. Ford, M. Kulmala, Revised parametrization of the Dillmann–Meier theory of homogeneous nucleation. *Phys. Rev. E Stat. Phys. Plasmas Fluids Relat. Interdiscip. Top.* **49**, 5517–5524 (1994).
36. K. K. Tanaka, H. Tanaka, T. Yamamoto, K. Kawamura, Molecular dynamics simulations of nucleation from vapor to solid composed of Lennard–Jones molecules. *J. Chem. Phys.* **134**, 204313 (2011).
37. R. Angélil, J. Diemand, K. K. Tanaka, H. Tanaka, Homogeneous SPC/E water nucleation in large molecular dynamics simulations. *J. Chem. Phys.* **143**, 064507 (2015).
38. I. Shim, K. A. Gingerich, Ab initio HF-CI calculations of the electronic "band structure" in the Fe_2 molecule. *J. Chem. Phys.* **77**, 2490–2497 (1982).

Acknowledgments: We thank N. Ishii and all project members of the sounding rocket S-520-28 experiment of the Japan Aerospace Exploration Agency (JAXA). **Funding:** This work was supported by a Grant-in-Aid for Scientific Research (S) from KAKENHI (15H05731), by a Grant-in-Aid for Young Scientists (A) from KAKENHI (24684033) of the Japan Society for the Promotion of Science, by a Grant-in-Aid for Scientific Research (C) from KAKENHI (2640023 and 15K05015), by a Grant-in-Aid for Scientific Research on Innovative Areas (16H00927), and by the Steering Committee for Space Biology and Microgravity Science of Institute of Space and Astronautical Science, JAXA. **Author contributions:** Y.K. designed the project, performed the experiments, and analyzed the data. K.K.T. performed the calculations. Y.K., K.K.T., and T.N. interpreted the data and cowrote the manuscript. Y.K., S.T., and Y.I. prepared the experimental system. S.T. and Y.I. prepared the interface between the experimental system and the sounding rocket. **Competing interests:** The authors declare that they have no competing interests. **Data and materials availability:** All data needed to evaluate the conclusions in the paper are present in the paper and/or the Supplementary Materials. Additional data related to this paper may be requested from the authors.

Submitted 23 August 2016
Accepted 30 November 2016
Published 18 January 2017
10.1126/sciadv.1601992

Citation: Y. Kimura, K. K. Tanaka, T. Nozawa, S. Takeuchi, Y. Inatomi, Pure iron grains are rare in the universe. *Sci. Adv.* **3**, e1601992 (2017).